NeuroImage 65 (2013) 522–528

Contents lists available at SciVerse ScienceDirect

NeuroImage

journal homepage: www.elsevier.com/locate/ynimg

Multispectral Opto-acoustic Tomography (MSOT) of the Brain and Glioblastoma Characterization

Neal C. Burton [a,b], Manishkumar Patel [c], Stefan Morscher [a,b,d], Wouter H.P. Driessen [a,b], Jing Claussen [a,b], Nicolas Beziere [a], Thomas Jetzfellner [a], Adrian Taruttis [a], Daniel Razansky [a,d], Bohumil Bednar [c], Vasilis Ntziachristos [a,d,*]

[a] Institute for Biological and Medical Imaging, Helmholtz Center Munich, Neuherberg, Germany
[b] iThera Medical, GmbH, Munich, Germany
[c] Merck Department of Imaging, West Point, Pennsylvania, USA
[d] Chair for Biological Imaging, Technical University of Munich, Munich, Germany

ARTICLE INFO

Article history:
Accepted 19 September 2012
Available online 28 September 2012

Keywords:
Multispectral opto-acoustic tomography
In vivo imaging
Nanoparticles
Glioblastoma
Brain

ABSTRACT

Brain research depends strongly on imaging for assessing function and disease *in vivo*. We examine herein multispectral opto-acoustic tomography (MSOT), a novel technology for high-resolution molecular imaging deep inside tissues. MSOT illuminates tissue with light pulses at multiple wavelengths and detects the acoustic waves generated by the thermoelastic expansion of the environment surrounding absorbing molecules. Using spectral unmixing analysis of the data collected, MSOT can then differentiate the spectral signatures of oxygenated and deoxygenated hemoglobin and of photo-absorbing agents and quantify their concentration. By being able to detect absorbing molecules up to centimeters deep in the tissue it represents an ideal modality for small animal brain imaging, simultaneously providing anatomical, hemodynamic, functional, and molecular information. In this work we examine the capacity of MSOT in cross-sectional brain imaging of mice. We find unprecedented optical imaging performance in cross-sectional visualization of anatomical and physiological parameters of the mouse brain. For example, the potential of MSOT to characterize ischemic brain areas was demonstrated through the use of a carbon dioxide challenge. In addition, indocyanine green (ICG) was injected intravenously, and the kinetics of uptake and clearance in the vasculature of the brain was visualized in real-time. We further found that multiparameter, multispectral imaging of the growth of U87 tumor cells injected into the brain could be visualized through the intact mouse head, for example through visualization of deoxygenated hemoglobin in the growing tumor. We also demonstrate how MSOT offers several compelling features for brain research and allows time-dependent detection and quantification of brain parameters that are not available using other imaging methods without invasive procedures.

Introduction

Neuroimaging has transformed brain research and clinical neurology by enabling early diagnosis of disease and critical feedback on the efficacy of treatments (Hargreaves, 2008; Wong et al., 2009). In addition, non-invasive imaging has enabled correlations between brain function and behavior (Logothetis, 2008). However, there is always a need to improve upon current technologies. Innovation, driven by assessing and offering alternatives to the limitations of current technologies, has and will continue to drive new discoveries in neuroimaging. There are currently many modalities available for neuroimaging, each with their own benefits and limitations. X-ray-based computed tomography (CT) and magnetic resonance imaging (MRI) provide anatomical information at high spatial resolution but with limited molecular specificity (Histed et al., 2012). On the other hand, positron emission tomography (PET) and fluorescence molecular tomography (FMT) are molecular imaging modalities (Ntziachristos and Razansky, 2010), but have low resolution. Intravital microscopy has molecular specificity at high resolution, but is limited by shallow tissue penetration and requires invasive procedures (Lichtman and Fraser, 2001).

We studied the performance of multispectral opto-acoustic tomography (MSOT) for neuroimaging in mice. MSOT combines the high resolution of anatomical techniques such as MRI, the molecular specificity of PET or FMT and the contrast of optical imaging to offer a highly potent

Abbreviations: MSOT, multispectral opto-acoustic tomography; FMT, fluorescence molecular tomography; NIR, near infrared; ICG, indocyanine green; X-ray CT, X-ray computerized tomography; MRI, magnetic resonance imaging; PET, positron emission tomography; FDA, food and drug administration; HEPES, 4-(2-hydroxyethyl)-1-piperazineethanesulfonic acid; i.v., intravascular.

* Corresponding author at: 1 Ingolstaedter Landstrasse, Building 56, Room 29, Neuherberg, 85764, Germany. Fax: +49 89 3187 3017.
E-mail address: v.ntziachristos@tum.de (V. Ntziachristos).

1053-8119/$ – see front matter © 2012 Published by Elsevier Inc.
http://dx.doi.org/10.1016/j.neuroimage.2012.09.053

modality that has been implemented recently for small animal imaging in real-time (Buehler et al., 2010; Ntziachristos and Razansky, 2010). It therefore offers several attractive characteristics for studying brain function and disease. Opto-acoustic imaging is based on the generation of acoustic waves following the absorption of light pulses of short (10–100 ns) duration by photo-absorbing molecules or nanoparticles. Transient absorption of light leads to a transient temperature increase in the mK range (Xiang et al., 2007) which in turn gives rise to a thermoelastic tissue expansion that produces ultrasonic waves. By detecting the acoustic waves using ultrasonic detectors and subsequent mathematical inversion, the distribution of optical absorption can be reconstructed in tissues with ultrasound imaging resolution, i.e. 20–200 μm. Single-wavelength images can yield anatomical information on the absorption contrast of different tissue structures. Illumination at multiple wavelengths and the spectral processing of the data captured can further lead to resolving spectral signatures of tissue molecules, extrinsically administered absorbing agents and nanoparticles with certain spectral signatures. Deoxygenated and oxygenated hemoglobin have substantial, unique absorptions in the NIR spectrum and therefore can be resolved with multispectral decomposition of opto-acoustic signals (Brecht et al., 2007; Esenaliev et al., 2002; Wang et al., 2006). Interestingly, injected agents can be distinguished from intrinsic absorbers. For example, perfusion of ICG through the kidney vasculature has previously been documented by MSOT (Buehler et al., 2010; Taruttis et al., 2012). Spectral separation (decomposition) also makes it possible to differentiate vascular MSOT signals derived from injected gold nanoparticles versus those derived from oxygenated and deoxygenated blood (Herzog et al., 2012; Taruttis et al., 2010). By illuminating at different wavelengths, spectrally tunable gold nanorods with different absorption maxima can simultaneously be detected *in vivo* (Li et al., 2008). Spectral shifts associated with molecular modifications can also be exploited for contrast generation. It was recently demonstrated that MSOT could visualize spectral modifications in response to NIR-probe activation by matrix metalloproteinases, detected *ex vivo* in human carotid arteries bearing atherosclerotic plaques (Razansky et al., 2012). In addition, sequential 2D slices can be compiled to produce volumetric quantitative molecular imaging in entire organs, small animals, or human tissues. The objective of the experiments herein is to evaluate the performance of MSOT and the potential utility of this technology in the investigation of molecular imaging biomarkers in diseases of the central nervous system.

Methods

Animals

Eight week old female nude CD-1 mice were used in compliance with the Helmholtz Zentrum Muenchen animal care and use committee for brain imaging and stereotactic implantation of U87 glioblastoma cells expressing firefly luciferase (1×10^5 cells in the striatum: Bregma +0.5 mm, lateral 2.0 mm, depth 3.0 mm). During continuous imaging of blood oxygenation with lethal anesthesia, mice were euthanized by carbon dioxide asphyxiation. For injection of contrast agents into the dorsal 3rd ventricle, the injection was performed stereotactically at Bregma −0.2 mm at a depth of 3.0 mm. Animals are imaged under 1.8% isoflurane anesthesia, and the body temperature is maintained at 34 °C.

Imaging agents

Indocyanine green (ICG) (Pulsion Medical Systems, Germany) was selected due to its well-studied fluorescence and opto-acoustic properties. It is an FDA-approved, water-soluble, inert anionic tricarbocyanine dye. For the *in vivo* study of ICG kinetics, 50 nmol of ICG was injected i.v. in 200 μl. For injections into the dorsal third ventricle, ICG-containing liposomes (0.4 mM ICG, 20 μM lipid) were provided by iThera Medical, GmbH (Neuherberg, Germany). Two microliters were injected directly into the brain.

Experimental MSOT imaging system

The experimental MSOT setup used has been described elsewhere (Buehler et al., 2010; Taruttis et al., 2010). A tunable optical parametric oscillator pumped by an Nd:YAG laser (Phocus, Opotek Inc., Carlsbad, CA) provides excitation from 680 nm to 950 nm. The laser pulse duration is below 10 ns and the pulse repetition frequency is 10 Hz. The tuning time between wavelengths for the laser is 2–3 s. The beam is coupled into a custom fiber bundle (CeramOptic Industries, Inc., East Longmeadow, MA) that is divided into 10 output arms, which serve to illuminate the mouse evenly from multiple angles on the imaging plane. A custom-made piezocomposite ultrasonic cylindrically-focused transducer array (Imasonic SAS, Voray, France) with 64 elements having a central frequency of 5 MHz (55% bandwith) is used for detection. The individual elements are 15 mm in width, and arranged in a 172° array with a focal distance and radius of 40 mm. The transducer array and fiber bundle outputs are submerged in a water bath maintained at 34 °C. Mice are placed in a horizontal position in a holder under isoflurane anesthesia with a thin polyethylene membrane with no direct contact between water and the mouse. This arrangement allows acoustic coupling between the mouse being imaged and the transducer array. The laser beams and ultrasonic transducer array are in fixed position for all data acquisitions, whereas the mouse can be translated through the imaging plane using a linear stage (NRT 150/M, Thorlabs GmbH, Dachau, Germany) to enable imaging of multiple transverse slices. The resolution of the translational stage is 0.1 mm. With one exception, the following wavelengths were used in all acquisitions: 700 nm, 730 nm, 760 nm, 800 nm, 860 nm, 900 nm. In the video-rate acquisition of ICG accumulation in the brain, 800 nm, the wavelength of maximum absorption for ICG, was used.

Image processing

Images were reconstructed using the interpolated model-matrix inversion (Rosenthal et al., 2010), where the main advantage of the method compared to state-of-the-art backprojection algorithms lies in its ability to include advanced effects of the transducer geometry in the reconstructed image. It can thus cope better with the extreme limited view scenario encountered in the case of the 172° transducer array used here, reducing the impact of artifacts in order to enable more quantitative imaging. After image reconstruction, linear spectral un-mixing was applied to detect signals from photo-absorbing tissue elements, such as hemoglobin or ICG (Razansky et al., 2009). For each pixel in the image, the method fits the total measured opto-acoustic spectrum to the known absorption spectra of oxy- and deoxy-hemoglobin and that of the agent to be detected. The MSOT data for the ICG kinetic study was fitted to a two-compartment open body model using WinNonLin (Pharsight, Munich, Germany).

Cryosectioning with fluorescence image acquisition

For whole-body, *ex vivo*, cross-sectional fluorescence imaging of probe biodistribution, a Leica cryoslicer (CM 1950, Leica Microsystems, GmbH, Wetzler, Germany) was retrofitted with a custom-made fluorescence imaging system (Sarantopoulos et al., 2011) with excitation at 740 nm and emission captured with a 780 long pass filter. This setup allows the user to acquire RGB and fluorescence images of the tissue specimen in the cryostat (i.e. whole body distribution can be documented by acquiring sequential images as the animal is sectioned). To provide an anatomical reference for MSOT images, animals were imaged by MSOT, euthanized, frozen intact and then sectioned/imaged.

Results

In vivo MSOT brain imaging and pharmacokinetic modeling

A CD1 nude mouse was used to examine the relative attenuation and effects of skin and skull on opto-acoustic *in vivo* brain imaging. Figs. 1A–C show single wavelength MSOT images acquired at 800 nm through intact skin and skull at different coronal slices of the brain (Bregma 0.26 mm, −0.94 mm and −2.18 mm, respectively), while Fig. 1D serves as an anatomical reference at Bregma −2.18 mm. Brain structures such as the superior sagittal sinus (solid arrow), the third ventricle (dotted arrow), and the posterior cerebral arteries (arrow with long dashes), deep within the brain, seen in the reference anatomy, can also be seen by MSOT through intact skin and skull. Other prominent sources of signals arise from the superficial temporal arteries (arrow with short dashes) outside of the brain.

To examine the ability to visualize dynamics and brain perfusion, ICG was injected into the tail vein and the uptake and clearance of ICG was monitored by MSOT in the vasculature of the head and brain dynamically and in real-time. ICG does not cross the blood

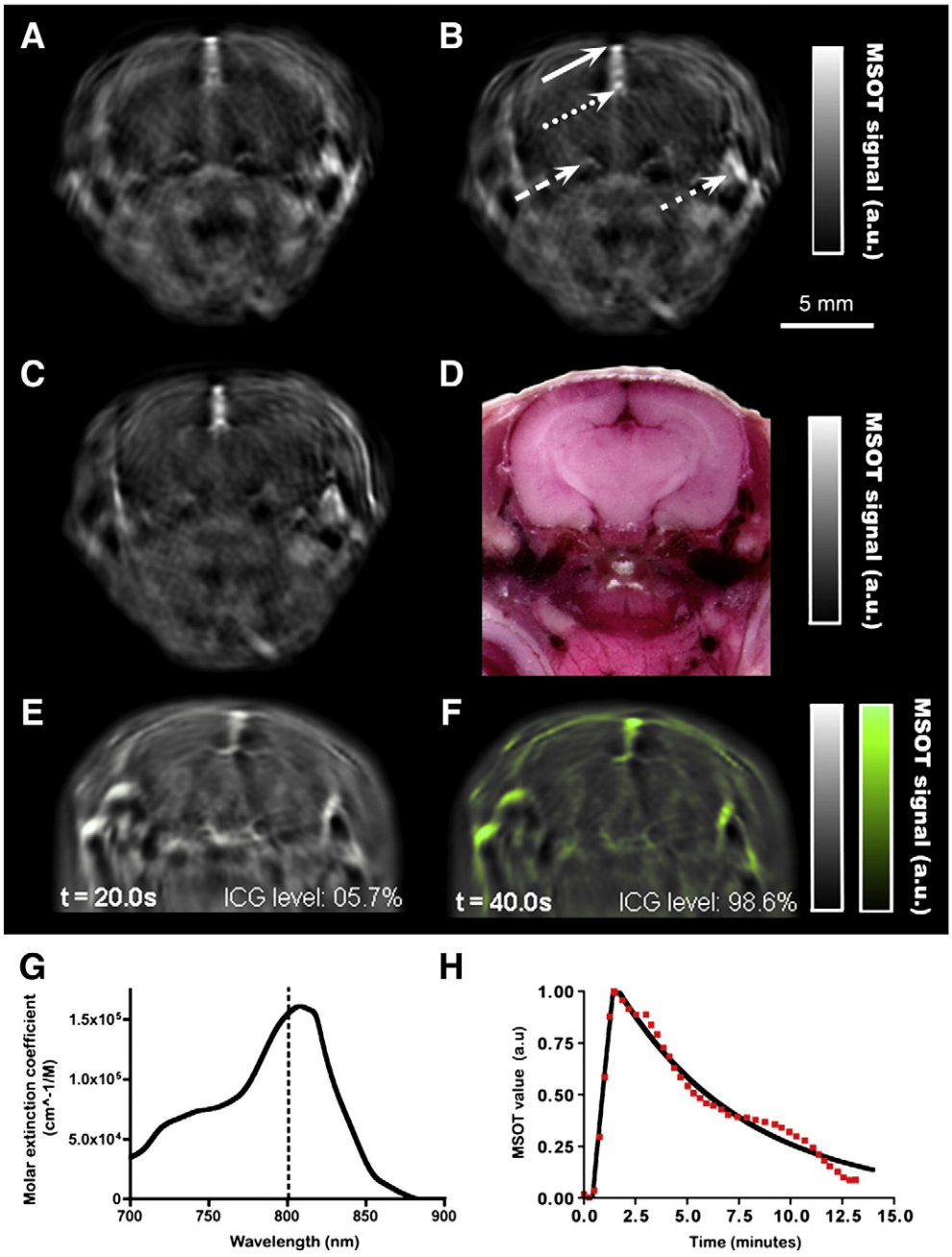

Fig. 1. *In vivo* MSOT brain imaging and pharmacokinetic modeling. Single wavelength (800 nm) anatomical opto-acoustic images of an intact brain from a living mouse (panels A–C, at Bregma 0.26 mm, −0.94 mm and −2.18 mm, respectively). In panel B, brain structures such as the superior sagittal sinus (solid arrow), the third ventricle (dotted arrow), and the posterior cerebral arteries (arrow with long dashes), and the superficial temporal arteries (arrow with short dashes) can be seen. Panel D shows reference anatomy from a frozen sectioned mouse at Bregma −2.18 mm. In panels E–H, 50 nm of indocyanine green was injected into the tail vein of a CD1 nude mouse and the uptake of ICG in the vasculature of the brain was monitored in real-time by MSOT. Panels E and F show a single wavelength opto-acoustic anatomical image (grayscale) 5 s prior to injection (panel E) and 40 s after injection (panel F) with the increase in optoacoustic amplitude shown in green. Panel G shows the absorption spectrum of ICG with the wavelength used in the acquisition of experimental data, 800 nm, shown as a dashed line. Panel H shows the quantification of ICG signal in the superior sagittal sinus during 14 min following injection, with experimental data in red and modeled data in black.

brain barrier; therefore, the increase in signal following injection is expected to be transient. Figs. 1E and F show representative MSOT images, with a single wavelength 800 nm MSOT image before injection (panel 1E) and the increased signal over baseline 40 s following injection shown in green (panel 1 F). Fig. 1G shows the absorption spectrum of ICG, with the dashed line indicating the near-maximal wavelength at which the experiment was performed. Fig. 1H shows the measured increase and subsequent decrease in ICG signal in the superior sagittal sinus over time. The red data points represent a subset of the acquired data points (for data presentation, the data is not depicted as it was acquired at 10 Hz), while the black curve shows the modeled data. The half-life of the initial clearance phase was 4.3 min and of the secondary phase 23.7 min, in good accordance with murine biliary excretion rates. This experiment was repeated in multiple animals and in multiple blood vessels throughout the body with comparable results (data not shown). The first 60 s of the experiment showing the rapid uptake of ICG into the vasculature of the brain is shown as Supplementary Video 1.

Brain blood oxygenation following carbon dioxide challenge

In further investigations into the utility of multispectral wavelength image acquisition in MSOT, we performed CO_2 pulse-chase experiments (CO_2 challenge) in mice because deoxygenated and oxygenated blood have distinct absorption spectra that can be accurately separated by spectral un-mixing methods. Mice were anesthetized with normal air and 1.5% isoflurane. While continuously acquiring multispectral measurements, the air mixture was successively changed (from normal air to 10% carbon dioxide, then to 100% oxygen, then to 100% carbon dioxide) to induce changes in oxygenation in the brain. Each multispectral measurement required approximately 25 s for acquisition. The multispectral data were then used to spectrally decompose the signals from oxy- and deoxy-hemoglobin in the superior sagittal sinus at each time point. Figs. 2A, B and C show deoxy-hemoglobin pseudocolor images from a single animal at 4.6, 6.2 and 9.6 min, respectively, with increasing deoxygenation depicted in blue. Figs. 2D, E and F show corresponding oxyhemoglobin in red at the same time points. Fig. 2G shows a merge of oxy- and deoxy-hemoglobin signals at 6.2 min (corresponding to Figs. 2B and E). Panels H and I plot the corresponding oxy- and deoxy-hemoglobin signals, respectively, throughout the experiment with dashed lines indicating the time-points for which images are shown. MSOT-derived oxy-hemoglobin measurements track the increase in inspired oxygen as well as the delivery of 100% carbon dioxide. MSOT-derived deoxy-hemoglobin measurements mirror those of oxy-hemoglobin.

Multispectral un-mixing of deoxyhemoglobin in glioblastoma and liposomal ICG distribution in brain

In the next experiment, 1×10^5 U87 human glioblastoma cells were injected into the striatum. At 34 days post implantation, the animal was scanned at multiple wavelengths by MSOT. The animal was then euthanized and the entire head was sectioned as a reference for MSOT and to verify the presence of a tumor (Fig. 3B). The reference cryoslice showed the presence of a large tumor in the right hemisphere. Following decomposition of multispectral data into a deoxygenated hemoglobin

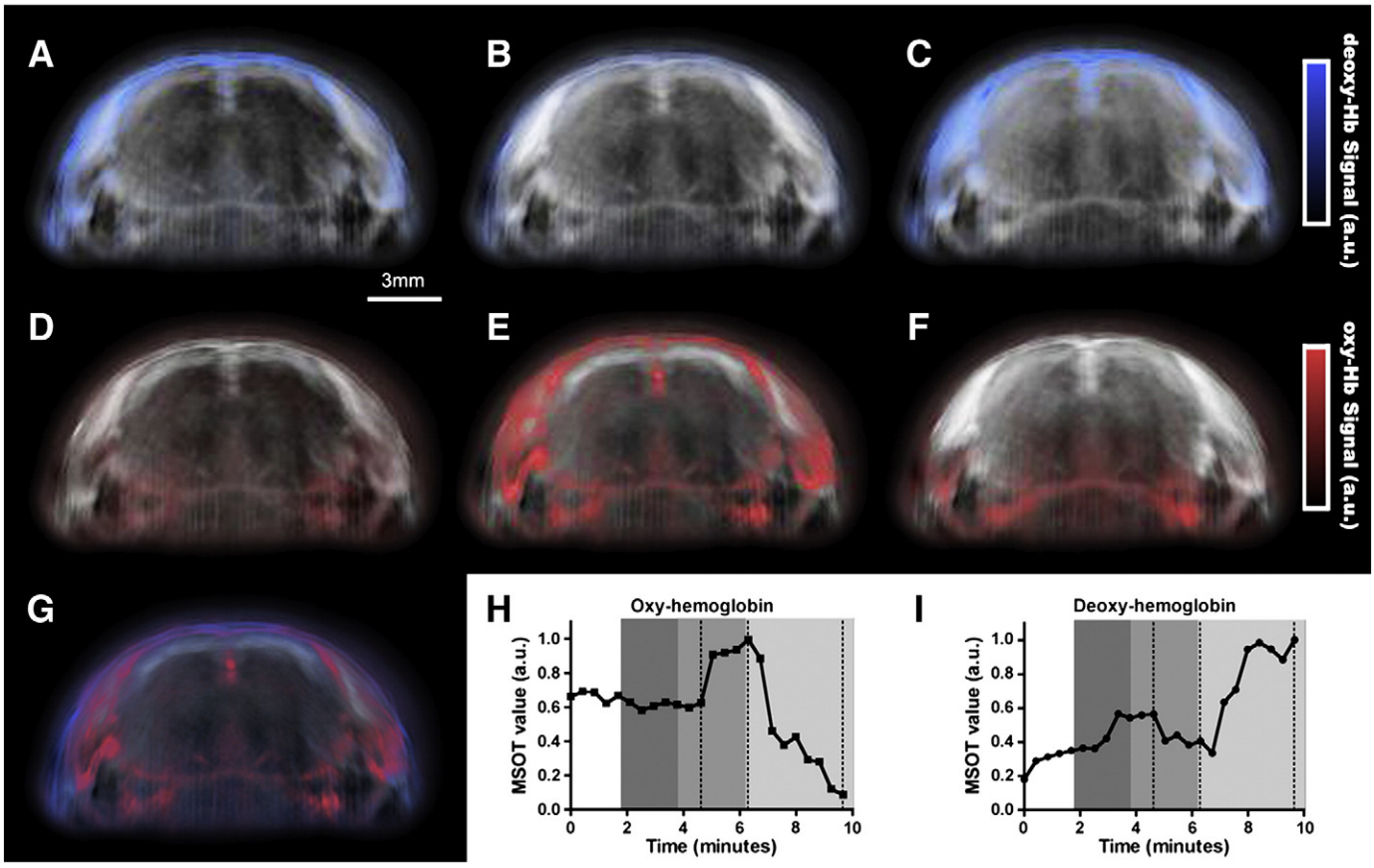

Fig. 2. Brain blood oxygenation following carbon dioxide challenge. While continuously acquiring multispectral measurements, the air mixture that the animal inspired was successively changed. The graphs in H and I are color-coded to show the temporal changes in inspired air (white, normal air; dark gray, 10% carbon dioxide; intermediate gray, 100% oxygen; and, light gray, 100% carbon dioxide). Panels A, B and C show deoxy-hemoglobin pseudocolor images from a single animal at 4.6, 6.2 and 9.6 min, respectively, with increasing deoxygenation depicted in blue. Panels D, E and F show corresponding oxyhemoglobin in red at the same time points. Panel G shows a combination of oxy- and deoxy-hemoglobin signals at 6.2 min (corresponding to panels B and E). Panels H and I plot the corresponding oxy- and deoxy-hemoglobin signals, respectively, throughout the experiment.

image (Fig. 3A), a strong correlation was observed in tumor location and size between the cryoslice and the deoxygenated hemoglobin signal. A close inspection of each of the images reveals an excellent correlation between substructures of the tumor in the MSOT and in the cryoslice images. Fig. 3C shows a deoxy-hemoglobin image 16 days following implantation. As an alternative approach to visualize the tumor, a similar carbon dioxide challenge was performed on the animal as described in Section 3.2 with the exception that mice were not given the final dose of 100% CO_2. Whereas the deoxy-hemoglobin signal was not sufficient to depict the tumor when the animal inspired 100% oxygen (data not shown), increasing the carbon dioxide concentration to 10% allowed the visualization of the tumor (Fig. 3C). Before the animal was euthanized, IntegriSense750 was injected to visualize the tumor. IntegriSense750 binds to angiogenic $\alpha_v\beta_3$ integrin receptors on the surface of cancer cells and absorbs in the NIR (Zhu et al., 2010). The brain was sectioned, and a fluorescence image was captured of the corresponding brain region. Panel 3D shows the tumor fluorescence in green overlaid onto an RGB image of the brain. There is an excellent correlation in the size, shape, and location of the tumor as assessed by fluorescence and (Fig. 3D) and MSOT (Fig. 3C) imaging.

In an investigation into multispectral wavelength acquisition with spectral decomposition of agents of interest, 2 μl of ICG encapsulated into liposomes was injected into the dorsal third ventricle of a mouse. The animal was scanned at multiple wavelengths in order to spectrally decompose the ICG signal. The fluorescence of ICG was used to validate the spatial distribution of the injected agent following cryosectioning and fluorescence imaging. Fig. 3E shows an opto-acoustic anatomical 800 nm image (grayscale) with an overlay (green) of the spectrally-resolved liposomal ICG signal. The MSOT image suggests that following injection into the dorsal third ventricle, the liposomes diffused into the third ventricle and the lateral ventricles. Fig. 3F shows the equivalent cryoslice with an overlay of the fluorescence from the injected particles. Overall, there was an excellent correlation in the spatial distribution of injected particles as shown by MSOT and *ex vivo* cryosectioning with fluorescence imaging.

Discussion and conclusion

Discussion

Opto-acoustic tomography has previously been utilized to perform brain imaging. Preliminary studies performed *ex vivo* showed the 3D distribution of oxygenated and deoxygenated blood in the brain using a single ultrasound transducer on a linear stage (Wang et al., 2003). The MSOT signal has previously been shown to have a linear dependence on brain blood oxygenation (Petrov et al., 2004). Subsequent brain MSOT studies in rodents *in vivo* have shown increased contrast in the superficial vasculature of the brain following ICG (Wang et al., 2004) or gold nanorod (Lu et al., 2010) injection. Finally, opto-acoustic tomography has previously been used to show a tumor-induced reduction in blood oxygenation in the superficial vasculature of the brain (Lungu et al., 2007).

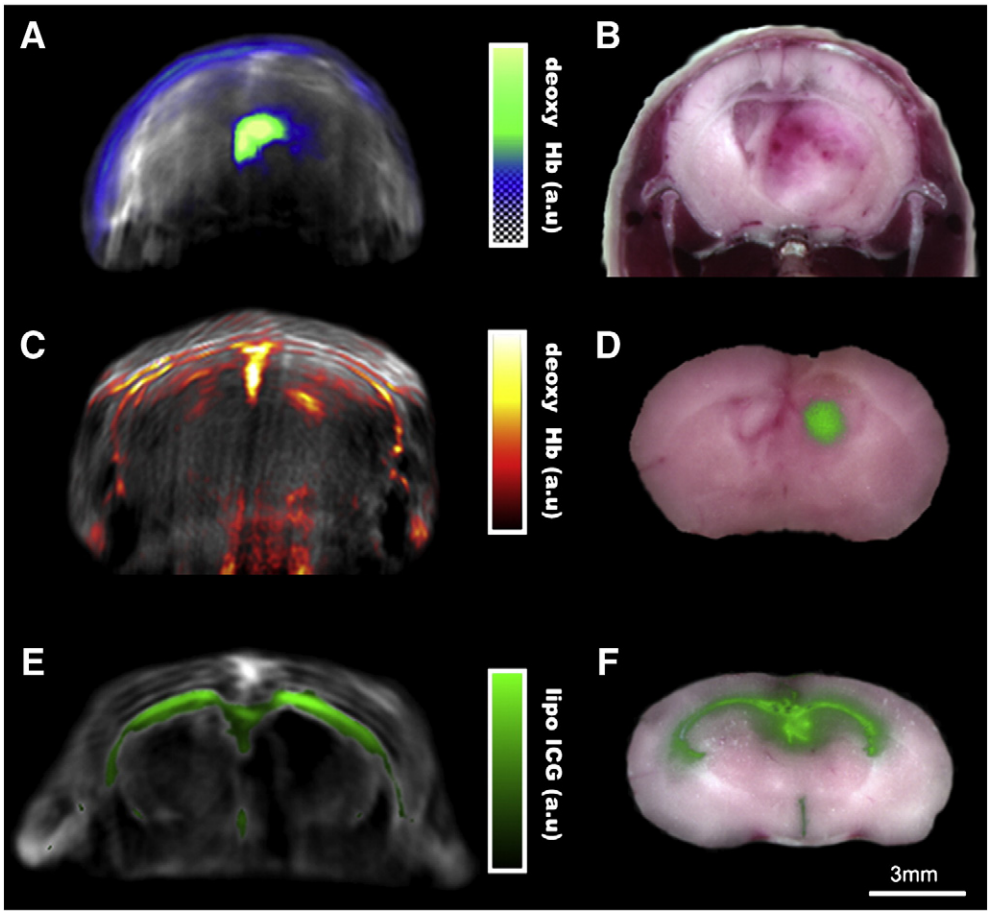

Fig. 3. Multispectral unmixing of glioblastoma and liposomal ICG distribution in brain. Panel A shows the spectrally unmixed deoxy-hemoglobin pseudocolor overlay on an 800 nm single wavelength MSOT image from an animal 34 days following implantation with U87 glioblastoma cells with a corresponding *ex vivo* cryosection in B. Panel C shows a deoxy-hemoglobin image 16 days following implantation following a 10% carbon dioxide challenge with corresponding ex vivo fluorescence image from IntegriSense750 showing tumor size and location (panel D). Panels E and F show a mouse injected intraventricularly with ICG encapsulated into liposomes. Panel E shows a 900 nm single wavelength MSOT image (grayscale) with an overlay (green) of the spectrally-resolved liposome-ICG signal. Panel F shows the equivalent cryoslice with an overlay of the fluorescence from the injected particles.

Whereas the previously described *in vivo* opto-acoustic tomography studies have provided horizontal images of the superficial vasculature of the brain, the current work considers an implementation which allows for cross-sectional (coronal) imaging through the entire brain. It can therefore allow visualization of processes that involve various brain locations, at large field of view; analogous to small animal CT or MRI imaging. We have demonstrated that by employing opto-acoustic scanning implemented to provide axial images of mice, unprecedented optical imaging of structural and functional features in mouse brains was achieved. Previous *in vivo* brain opto-acoustic imaging studies have visualized only superficial brain features (Lu et al., 2010; Wang et al., 2004). Herein we show cross-sectional images through the entire depth of the mouse brain. Single wavelength images show detailed anatomical features such as the temporal arteries, and the superior sagittal sinus and deep blood vessels beneath the skull.

In addition to anatomical detail, MSOT also offers molecular and functional information. Deoxygenated and oxygenated hemoglobin have unique spectral absorptions in the near infrared, and account for the predominant intrinsic contrast (MSOT signal) in the images. Spectral un-mixing can be used to spatially resolve blood volume and oxygen saturation/hypoxia, a feature with significant implications in brain functional studies, disease development and evaluation of treatment Even though un-mixing of oxygenated and deoxygenated contributions has been previously documented using opto-acoustics, the work herein sheds new light on this analysis. Whereas previous work has shown brain blood oxygenation via opto-acoustics in sheep (Petrov et al., 2004), in mice *ex vivo* (Wang et al., 2003), or in mice *in vivo* in the superficial vasculature of the brain (Lungu et al., 2007), this work is the first example of the determination of brain oxygenation in a living mouse through the depth of the brain. This application was validated by continuously imaging an animal following a challenge with carbon dioxide. As expected, oxygenated hemoglobin dominates the MSOT signal when the animal receives 100% oxygen, whereas the predominant MSOT signal shifts to deoxygenated hemoglobin following carbon dioxide inspiration. Blood oxygenation was also utilized in a mouse model of glioblastoma to visualize the tumor. *Ex vivo* cryosectioning confirmed the presence of necrosis at the core of the late stage tumor. This hypoxic core was detectable through intact skin and skull by MSOT.

The use of a 5 MHz ultrasound transducer produces a resolution of approximately 150 μm, although higher resolution can be achieved when using higher frequencies. It would be possible to employ up to at least 30 MHz (~50 μm resolution) before ultrasound attenuation effects reduce the MSOT applicability to more superficial imaging. In addition to the high resolution achieved and the ability to resolve oxy- and deoxy-hemoglobin, several other unique features were found. MSOT was able to detect liposomal ICG injected into the ventricles of the brain which demonstrated the capacity of the technique to detect nanoparticles that could distribute throughout the animal's brain parenchyma. Much more work is required to determine the sensitivity in the detection of such novel multispectral nanoparticle-based probe systems within intact brain *in vivo*. Similarly the detection of ICG injected i.v. revealed the ability to detect organic photo-absorbing dyes in blood. Near infrared dyes represent potential MSOT contrast agents. Probes such as oxazine dyes (Hyde et al., 2009) that bind to amyloid plaques or the blood–brain barrier-permeable dye 3,3-diethylthiatricarbocyanine iodide (Wang et al., 2011), which binds with high specificity to myelin, or fluorescent proteins that absorb in the NIR (Filonov et al., 2011) could potentially be used to perform high-resolution longitudinal imaging with MSOT.

The data collected herein were acquired at 10 Hz, allowing for video-rate imaging. This permits the visualization of the kinetics of uptake and clearance of injected agents in the brain. This was demonstrated with an ICG tail vein injection with simultaneous MSOT imaging of the brain. ICG is not blood–brain barrier permeable; therefore, the dye transiently occupies the vasculature of the brain following injection. The MSOT data was fitted to a two-compartment open body model. This model was chosen because it has been established that the plasma ICG–concentration time curve shows a biphasic decay (Grainger et al., 1983; Meijer et al., 1988), with ICG rapidly eliminated from the blood (compartment 1) initially as it is taken up into peripheral tissues (compartment 2) and subjected to slower excretion kinetics. This experiment demonstrates the ability of MSOT to capture real-time events, such as the uptake of probe in the brain.

As this modality is non-invasive, it is possible to repeatedly scan individual animals, enabling longitudinal imaging. This feature can be exploited in a mouse model of glioblastoma to track tumor growth. At late stages in tumor growth, necrotic features of the tumor are evident following gross histological examination and can be visualized *in vivo* by MSOT as large areas of deoxygenation. However, at earlier stages, hypoxia without necrosis has been associated with tumor growth (Bar, 2011). The use of carbon dioxide challenges during MSOT measurement allows a reduction in global oxygenation in the brain with the resulting emphasis of hypoxic structures that would otherwise not be evident using 100% oxygen. This strategy is also used in functional MRI studies that utilize hypercapnic conditions (Liu et al., 2007) or medical air as opposed to 100% oxygen (Rauscher et al., 2005) to demonstrate changes in brain blood oxygenation. This method enables the detection via MSOT of the tumor *in vivo* through intact skin and skull, allowing an investigator access to molecular and functional features of tumor growth. With the development of blood–brain-barrier-permeable probes that absorb in the NIR, MSOT also has the potential to interrogate other molecular features of neurological disease.

Conclusion

In summary, MSOT brings important new features into small animal brain imaging. It was demonstrated herein that anatomical and physiological parameters were visualized in high resolution through brain cross-sections. This imaging capacity is in analogy to other high-resolution radiological modalities, also visualizing throughout the entire brain volume, but with the added ability to directly resolve oxygenated and deoxygenated hemoglobin and multispectral optical agents while following dynamic effects in real-time. This imaging ability may bring a new dimension in small animal brain research by allowing imaging of physiological and possibly molecularly targeted signals with high resolution; a capacity not available with optical or nuclear imaging techniques. In addition, multiple molecules can be visualized simultaneously; besides oxy- and deoxy-hemoglobin several more dyes and photo-absorbing nanoparticles can be multiplexed for concurrent imaging. We expect that the combination of the imaging performance exhibited by small animal MSOT together with new molecular probes will enable new insights into brain function and disease.

Supplementary data to this article can be found online at http://dx.doi.org/10.1016/j.neuroimage.2012.09.053.

Acknowledgment

We acknowledge support from the German Federal Ministry of Education and Research (BMBF) through the GO-Bio program.

References

Bar, E.E., 2011. Glioblastoma, cancer stem cells and hypoxia. Brain Pathol. 21, 119–129.
Brecht, H.P., Prough, D.S., Petrov, Y.Y., Patrikeev, I., Petrova, I.Y., Deyo, D.J., Cicenaite, I., Esenaliev, R.O., 2007. *In vivo* monitoring of blood oxygenation in large veins with a triple-wavelength optoacoustic system. Opt. Express 15, 16261–16269.
Buehler, A., Herzog, E., Razansky, D., Ntziachristos, V., 2010. Video rate optoacoustic tomography of mouse kidney perfusion. Opt. Lett. 35, 2475–2477.
Esenaliev, R.O., Larina, I.V., Larin, K.V., Deyo, D.J., Motamedi, M., Prough, D.S., 2002. Optoacoustic technique for noninvasive monitoring of blood oxygenation: a feasibility study. Appl. Opt. 41, 4722–4731.
Filonov, G.S., Piatkevich, K.D., Ting, L.M., Zhang, J., Kim, K., Verkhusha, V.V., 2011. Bright and stable near-infrared fluorescent protein for *in vivo* imaging. Nat. Biotechnol. 29, 757–761.

Grainger, S.L., Keeling, P.W., Brown, I.M., Marigold, J.H., Thompson, R.P., 1983. Clearance and non-invasive determination of the hepatic extraction of indocyanine green in baboons and man. Clin. Sci. (Lond.) 64, 207–212.
Hargreaves, R.J., 2008. The role of molecular imaging in drug discovery and development. Clin. Pharmacol. Ther. 83, 349–353.
Herzog, E., Taruttis, A., Beziere, N., Lutich, A.A., Razansky, D., Ntziachristos, V., 2012. Optical imaging of cancer heterogeneity with multispectral optoacoustic tomography. Radiology 263, 461–468.
Histed, S.N., Lindenberg, M.L., Mena, E., Turkbey, B., Choyke, P.L., Kurdziel, K.A., 2012. Review of functional/anatomical imaging in oncology. Nucl. Med. Commun. 33, 349–361.
Hyde, D., de Kleine, R., MacLaurin, S.A., Miller, E., Brooks, D.H., Krucker, T., Ntziachristos, V., 2009. Hybrid FMT-CT imaging of amyloid-beta plaques in a murine Alzheimer's disease model. Neuroimage 44, 1304–1311.
Li, P.C., Wang, C.R., Shieh, D.B., Wei, C.W., Liao, C.K., Poe, C., Jhan, S., Ding, A.A., Wu, Y.N., 2008. *In vivo* photoacoustic molecular imaging with simultaneous multiple selective targeting using antibody-conjugated gold nanorods. Opt. Express 16, 18605–18615.
Lichtman, J.W., Fraser, S.E., 2001. The neuronal naturalist: watching neurons in their native habitat. Nat. Neurosci. 4, 1215–1220 (Suppl.).
Liu, Y.J., Juan, C.J., Chen, C.Y., Wang, C.Y., Wu, M.L., Lo, C.P., Chou, M.C., Huang, T.Y., Chang, H., Chu, C.H., Li, M.H., 2007. Are the local blood oxygen level-dependent (BOLD) signals caused by neural stimulation response dependent on global BOLD signals induced by hypercapnia in the functional MR imaging experiment? Experiments of long-duration hypercapnia and multilevel carbon dioxide concentration. AJNR Am. J. Neuroradiol. 28, 1009–1014.
Logothetis, N.K., 2008. What we can do and what we cannot do with fMRI. Nature 453, 869–878.
Lu, W., Huang, Q., Ku, G., Wen, X., Zhou, M., Guzatov, D., Brecht, P., Su, R., Oraevsky, A., Wang, L.V., Li, C., 2010. Photoacoustic imaging of living mouse brain vasculature using hollow gold nanospheres. Biomaterials 31, 2617–2626.
Lungu, G.F., Li, M.L., Xie, X., Wang, L.V., Stoica, G., 2007. *In vivo* imaging and characterization of hypoxia-induced neovascularization and tumor invasion. Int. J. Oncol. 30, 45–54.
Meijer, D.K., Weert, B., Vermeer, G.A., 1988. Pharmacokinetics of biliary excretion in man. VI. Indocyanine green. Eur. J. Clin. Pharmacol. 35, 295–303.
Ntziachristos, V., Razansky, D., 2010. Molecular imaging by means of multispectral optoacoustic tomography (MSOT). Chem. Rev. 110, 2783–2794.
Petrov, Y., Prough, D., Deyo, D., Petrova, I., Motamedi, M., Esenaliev, R., 2004. *In vivo* noninvasive monitoring of cerebral blood with optoacoustic technique. Conf. Proc. IEEE Eng. Med. Biol. Soc. 3, 2052–2054.
Rauscher, A., Sedlacik, J., Barth, M., Haacke, E.M., Reichenbach, J.R., 2005. Nonnvasive assessment of vascular architecture and function during modulated blood oxygenation using susceptibility weighted magnetic resonance imaging. Magn. Reson. Med. 54, 87–95.
Razansky, D., Baeten, J., Ntziachristos, V., 2009. Sensitivity of molecular target detection by multispectral optoacoustic tomography (MSOT). Med. Phys. 36, 939–945.
Razansky, D., Harlaar, N.J., Hillebrands, J.L., Taruttis, A., Herzog, E., Zeebregts, C.J., van Dam, G.M., Ntziachristos, V., 2012. Multispectral optoacoustic tomography of matrix metalloproteinase activity in vulnerable human carotid plaques. Mol. Imaging Biol. 14 (3), 277–285.
Rosenthal, A., Razansky, D., Ntziachristos, V., 2010. Fast semi-analytical model-based acoustic inversion for quantitative optoacoustic tomography. IEEE Trans. Med. Imaging 29, 1275–1285.
Sarantopoulos, A., Themelis, G., Ntziachristos, V., 2011. Imaging the bio-distribution of fluorescent probes using multispectral epi-illumination cryoslicing imaging. Mol. Imaging Biol. 13, 874–885.
Taruttis, A., Herzog, E., Razansky, D., Ntziachristos, V., 2010. Real-time imaging of cardiovascular dynamics and circulating gold nanorods with multispectral optoacoustic tomography. Opt. Express 18, 19592–19602.
Taruttis, A., Morscher, S., Burton, N.C., Razansky, D., Ntziachristos, V., 2012. Fast multispectral optoacoustic tomography (MSOT) for dynamic imaging of pharmacokinetics and biodistribution in multiple organs. PLoS One 7, e30491.
Wang, X., Pang, Y., Ku, G., Stoica, G., Wang, L.V., 2003. Three-dimensional laser-induced photoacoustic tomography of mouse brain with the skin and skull intact. Opt. Lett. 28, 1739–1741.
Wang, X., Ku, G., Wegiel, M.A., Bornhop, D.J., Stoica, G., Wang, L.V., 2004. Noninvasive photoacoustic angiography of animal brains *in vivo* with near-infrared light and an optical contrast agent. Opt. Lett. 29, 730–732.
Wang, X., Xie, X., Ku, G., Wang, L.V., Stoica, G., 2006. Noninvasive imaging of hemoglobin concentration and oxygenation in the rat brain using high-resolution photoacoustic tomography. J. Biomed. Opt. 11, 024015.
Wang, C., Wu, C., Popescu, D.C., Zhu, J., Macklin, W.B., Miller, R.H., Wang, Y., 2011. Longitudinal near-infrared imaging of myelination. J. Neurosci. 31, 2382–2390.
Wong, D.F., Tauscher, J., Grunder, G., 2009. The role of imaging in proof of concept for CNS drug discovery and development. Neuropsychopharmacology 34, 187–203.
Xiang, L., Xing, D., Gu, H., Yang, D., Yang, S., Zeng, L., Chen, W.R., 2007. Real-time optoacoustic monitoring of vascular damage during photodynamic therapy treatment of tumor. J. Biomed. Opt. 12, 014001.
Zhu, L., Niu, G., Fang, X., Chen, X., 2010. Preclinical molecular imaging of tumor angiogenesis. Q. J. Nucl. Med. Mol. Imaging 54, 291–308.